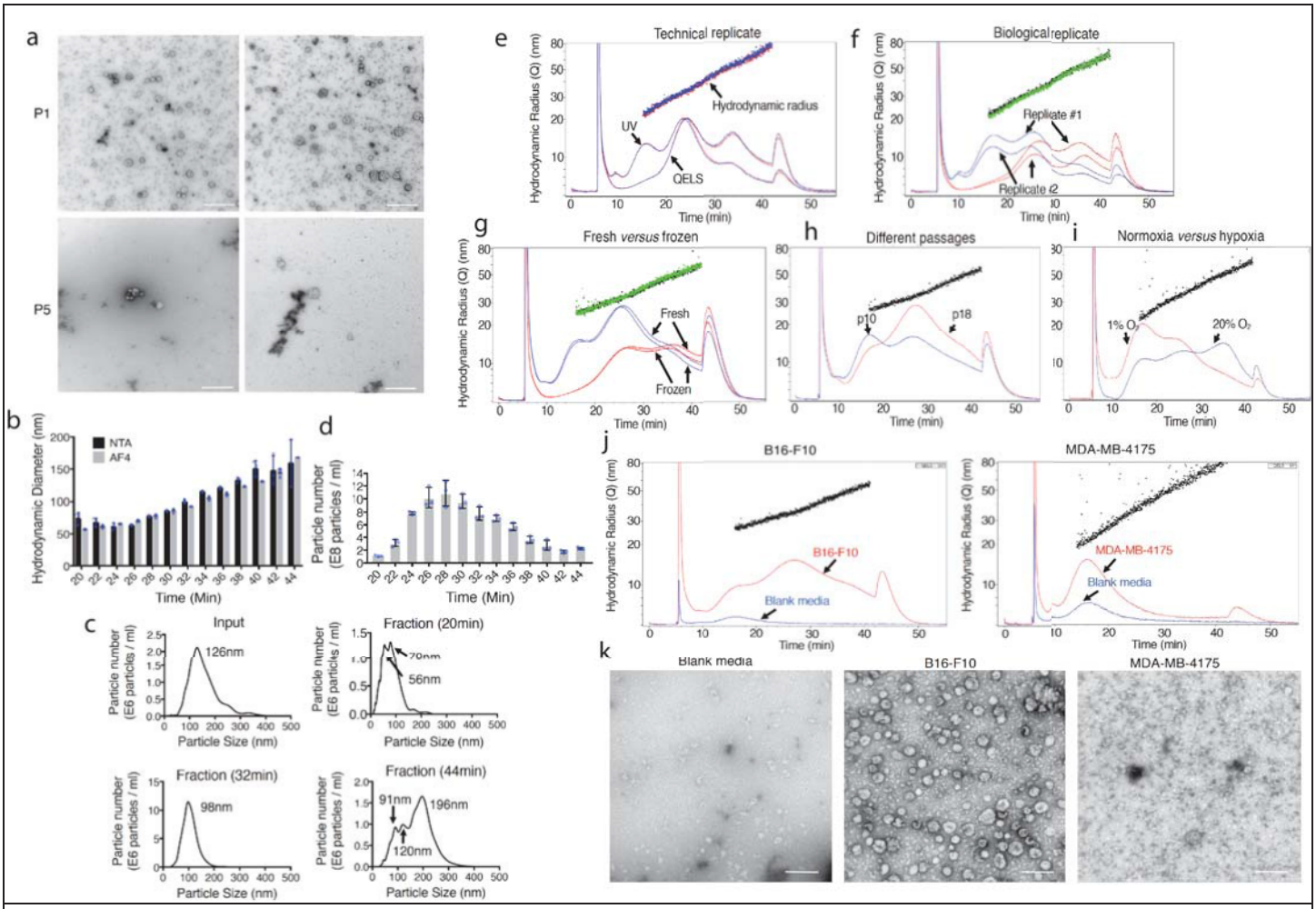

Supplementary Figure 1

Characterization of AF4 fractions using TEM imaging and NTA analyses and examination of AF4 profiles of nanoparticles derived from cells under different culture and storage conditions.

(**a**) TEM analysis of particles in AF4 peaks P1 and P5 of B16-F10. The experiment was repeated independently 3 times with similar result. Scale bar, 500 nm. (**b**) Comparison of the hydrodynamic diameter of each fraction determined by AF4-QELS *versus* NTA. Individual fractions (time slice, 0.5 min/fraction) were taken every 2 min from 20 to 44 min during the AF4 time course, and subjected to NTA. Results shown are mean ± SEM (n=3 independent samples). Mode size from NTA was utilized. X-axis, time course of AF4 (min); Y-axis, hydrodynamic diameter (nm). (**c**) The size distribution profiles of representative fractions by NTA (input, unfractionated samples; fractions at 20, 32, and 44 min). Multiple peaks were detected for fractions at 20 and 44 min by NTA. a mode size of 126 nm of Input indicates that NTA cannot efficiently resolve polydisperse samples and is biased towards large particles. This experiment was repeated 3 times independently with similar results. (**d**) Particle concentration of each fraction measured by NTA. The hydrodynamic diameter of the peak fraction (28 min) was 77nm. Results shown are mean ± SEM (n=3 independent samples). (**e-i**) AF4 profiles of B16-F10 sEVs collected from technical (blue lines, replicate #1; red lines, replicate #2) (**e**) and biological replicates (red lines, QELS; blue lines, UV; black (replicate #1) and green dots (replicate #2), hydrodynamic radius; Differences in UV and QELS signal intensity is due to the different amount of input samples for two replicates) (**f**), kept at either 4 ^{o}C or -80 ^{o}C for one week (red lines, QELS; blue lines, UV; black (fresh) and green dots (frozen), hydrodynamic radius) (**g**), cells of different passage numbers (blue and red lines, UV of cells at passage 10 and 18, respectively; black dots, hydrodynamic radius) (**h**), and under hypoxic *versus* normoxic conditions for 48 h (blue and red lines, UV for samples cultured with 20% and 1% O_2, respectively; black dots, hydrodynamic radius) (**i**). Experiments were repeated independently 3 times for (**e-g**) and twice for (**h**) with similar results. For (**i**), the experiment was repeated with 3 different cell lines independently with similar results. (**j**) AF4 and (**k**) TEM analysis of nanoparticles isolated in parallel from the blank media control and CM of 3-day cultures of B16-F10 and MDA-MB-4175. This experiment was done once. (Red and Blue lines, UV; black dots, hydrodynamic radius; Scale bar, 200 nm.) Statistical source data are provided in Supplementary Table 8.

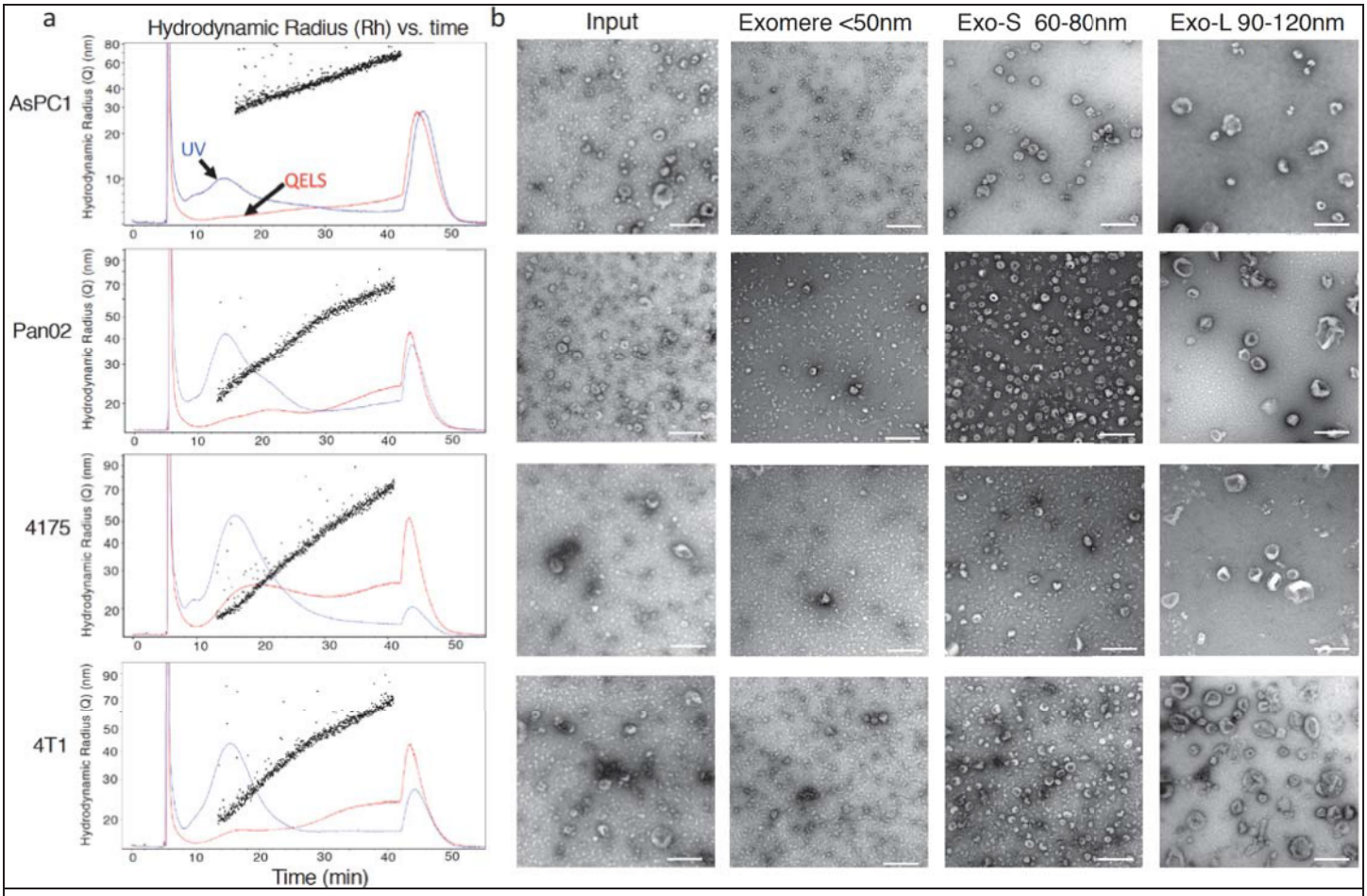

Supplementary Figure 2

Identification of exomeres and exosome subpopulations released by multiple cancer cell lines.

Shown are AF4 profiles (**a**) and representative TEM images (**b**) of unfractionated input samples and pooled fractions of exomeres, Exo-S and Exo-L that derived from various cancer cell lines, including AsPC1, Pan02, MDA-MB-4175, and 4T1. Multiple independent experiments were conducted with similar results for (**a**) (repeated times: AsPC-1, 9x; Pan02, 16x; 4175, 17x; 4T1, 10x) and (**b**) (AsPC-1, 3x; Pan02, 2x; 4175, 1x; 4T1, 4x). Scale bar, 200 nm. x- axis, time (min); y-axis (scale) and black dots, hydrodynamic radius (nm); Red and blue lines illustrate the QELS (DLS) intensity and UV absorbance (shown on a relative scale), respectively.

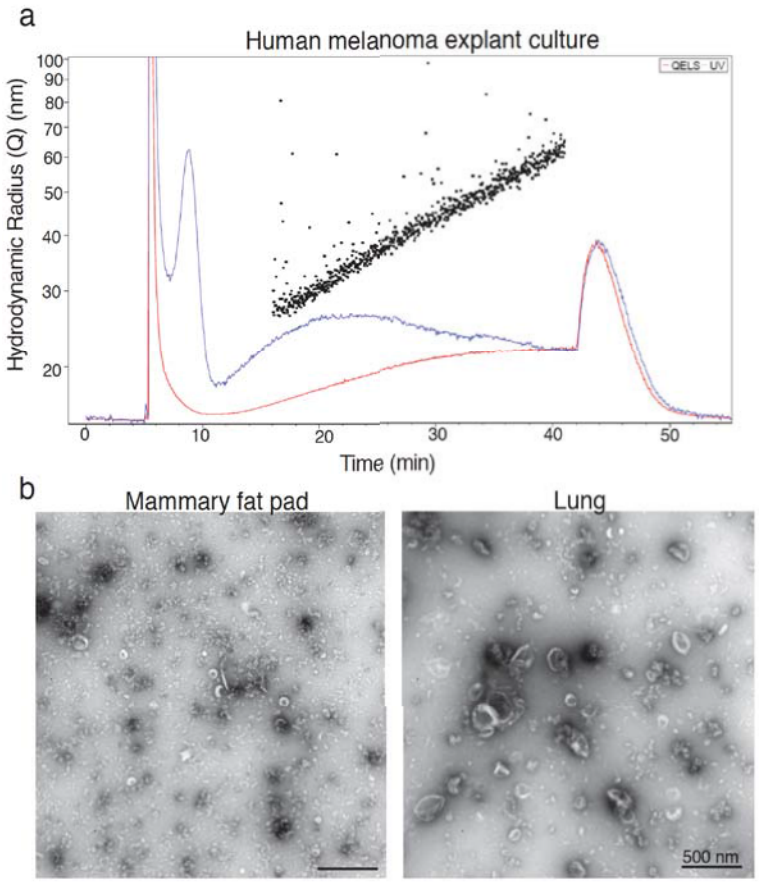

Supplementary Figure 3

Detection of exomeres, Exo-S and Exo-L in samples isolated from the tissue explant cultures.

(a) AF4 profile of exosomes isolated from explant culture of fresh human melanoma tissues. Red and blue lines illustrate the QELS (DLS) intensity and UV absorbance, respectively. This experiment was repeated with 4 independent specimens with similar results. **(b)** TEM images of exosome samples isolated from the explant culture of normal mouse mammary fat pad and lung tissues. This experiment was repeated independently 2 times with similar results. Scale bar, 500 nm.

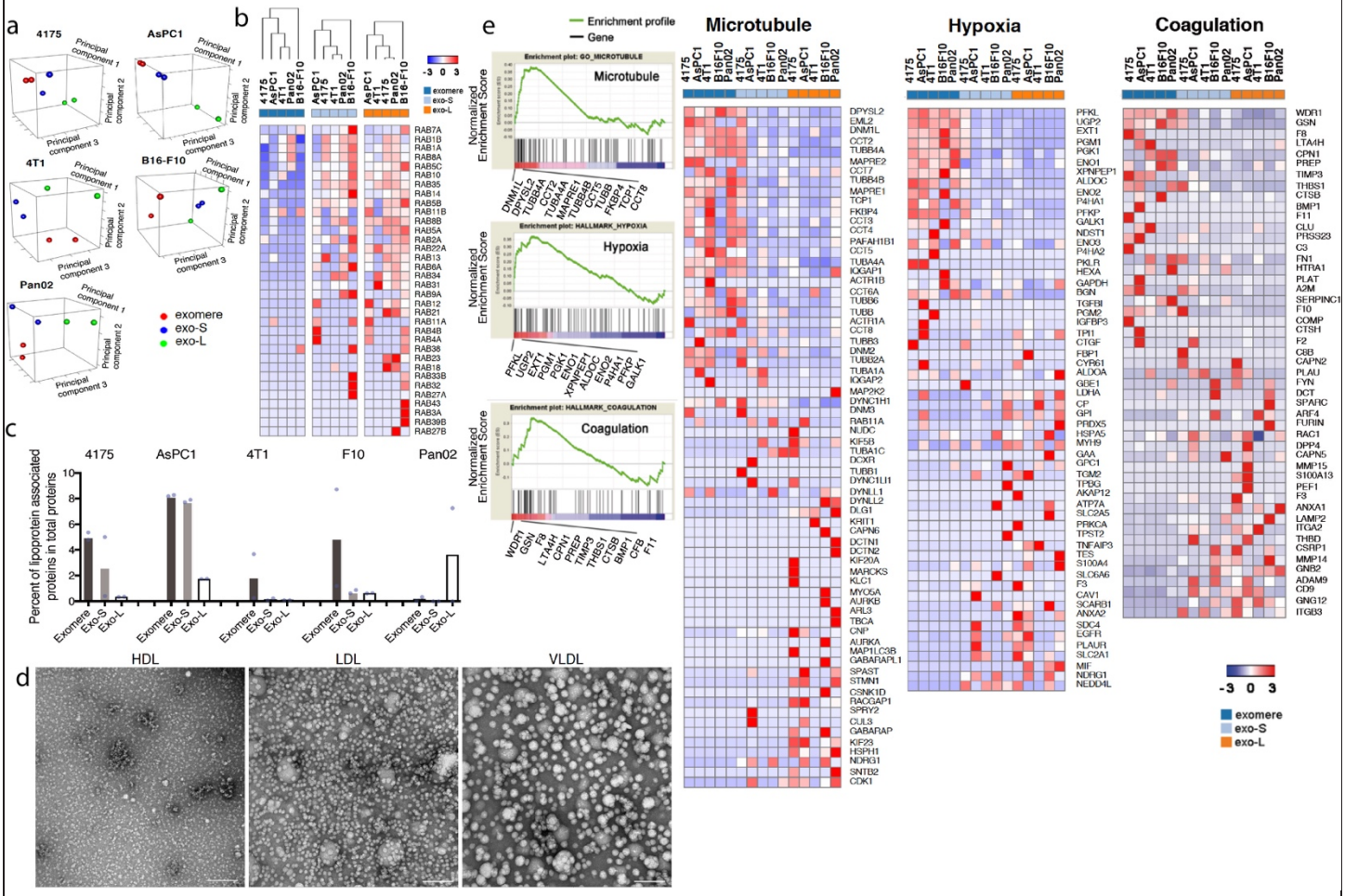

Supplementary Figure 4

Proteomic profiling of exomeres and exosome subpopulations derived from multiple cancer cell lines.

(a) Principal component analysis of normalized proteomic mass spectrometry data of exomeres, Exo-S and Exo-L derived from multiple cell lines, including MDA-MB-4175, AsPC1, 4T1, B16F10 and Pan02. Two independent biological replicates were analyzed for each nanoparticle sample. **(b)** Heat map illustration of the relative abundance of the Rab family proteins in exomeres, Exo-S and Exo-L. Scale shown is intensity (area) subtracted by mean and divided by row standard deviation (i.e. Δ (area-mean)/SD). **(c)** Evaluation of the presence of lipoprotein-particle associated proteins (listed in Supplementary Table 5) among the total proteins detected in the exomere, Exo-S and Exo-L derived from different cell lines. Results shown are mean of 2 biologically independent experiments. Statistical source data are provided in Supplementary Table 8. (**d**) TEM imaging analysis of HDL, LDL and VLDL. Scale bar, 200 nm. This experiment was done once with multiple images showing similar results. **(e)** Identification of specific association of signaling pathways including hypoxia (FDR, q value = 0.004), microtubule (FDR, q value = 0.002) and coagulation (FDR, q value = 0.013) with exomeres by GSEA (left panel) and the heat map illustration of the expression level of related proteins in different subsets of nanoparticles (right panel). A total of n=30 samples (3 nanoparticle subtypes derived from 5 different cell lines; and two independent biological replicates for each nanoparticle samples) were subjected for Kolmogorov-Smirnov statistical analysis.

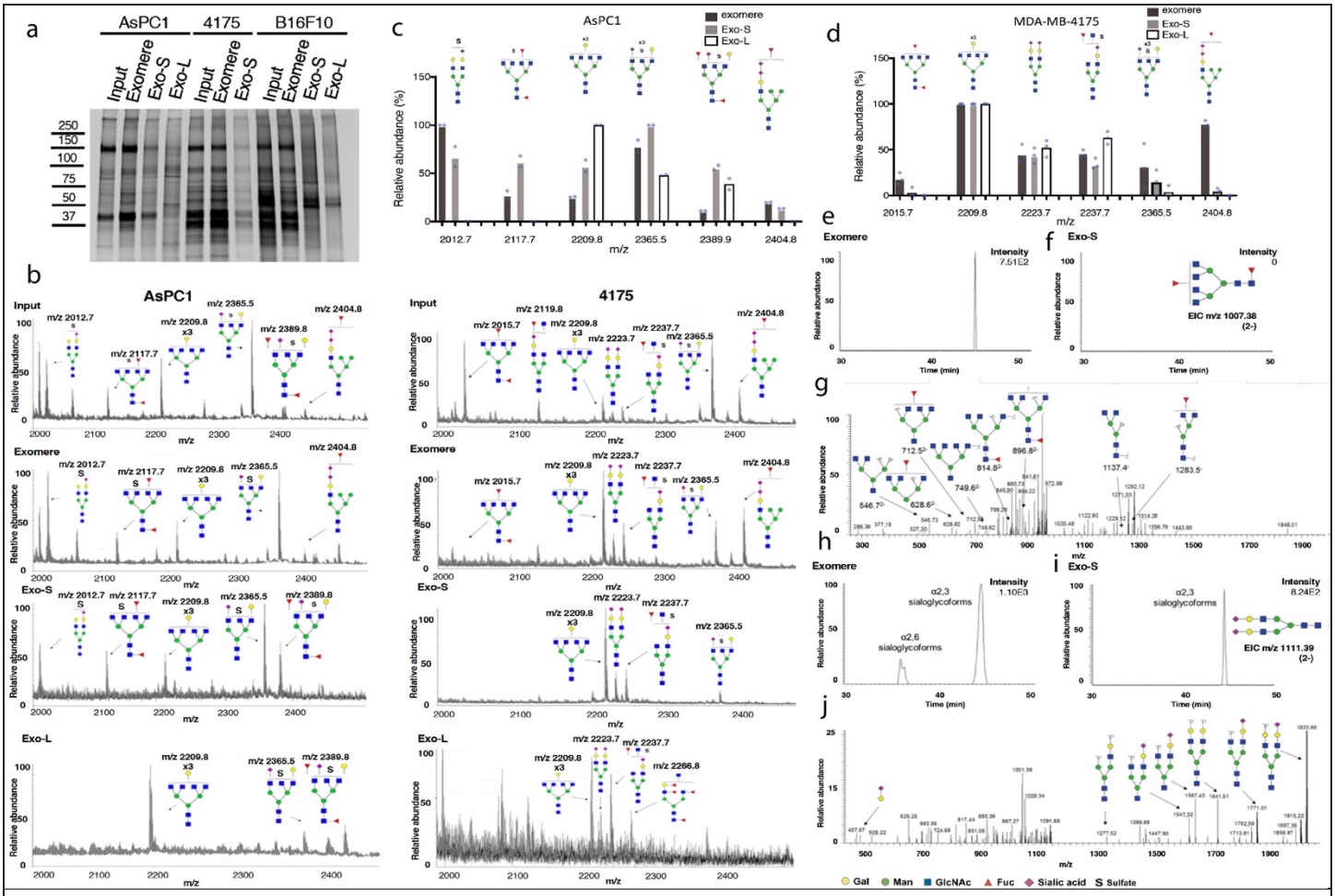

Supplementary Figure 5

Mass spectrometric analysis of *N*-glycans enriched in exomeres, Exo-S and Exo-L derived from AsPC1 and MDA-MB-4175.

(a) Total protein profile content of the isolated exomere, Exo-S and Exo-L subpopulations derived from AsPC-1, MDA-MB-4175 and B16-F10 assessed by silver staining. This experiment was repeated independently twice for B16-F10 and 4175 with similar results and done once for AsPC-1. (**b**) The *N*-glycan mass spectra of particles derived from AsPC-1 (left panel) and MDA-MB-4175 (right panel), respectively. This experiment was done once with 3 analytic replicates with similar results. (**c**) and (**d**) Quantification of the top six most abundant *N*-glycan structures identified in the study of AsPC1 and MDA-MB-4175 derived particles. Data shown were quantified and normalized to the most abundant structure in the sample. Results are represented as mean of 2 and 3 independent analytical measurements for AsPC-1 for MDA- MB-4175, respectively. NanoHPLC-PGC-HRMS extracted ion chromatograms (EIC) and CID-MS/MS spectra for **(e-g)** the ion at *m/z* 1007.38(2-), corresponding to a core-fucosylated complex type *N*-glycan, characteristic of exomere, and **(h-j)** the ion at *m/z* 1111.39(2-), corresponding to a disialylated complex-type *N*-glycan found in all fractions of B16F10. Fragmentation analysis for extracted ion chromatogram *m/z* 1007.38 (2-) confirming the structure of this *N*-glycan in exomeres (**e** and **g**) and demonstrating the absence of this *N*-glycan in Exo-S (**f**). According to the relative retention time on the PGC column, exomeres contain both α2,3-linked and α2,6-linked sialoglycoforms of the ions at *m/z* 1111.39(2-) (**h**). The *N*-glycan *m/z* 1111.39(2-) from Exo-S showed *N*-glycans displaying exclusively α2,3-linked sialic acids based on PGC-LC relative retention time (**i**). This experiment (**e-j**) was done once. Statistical source data are provided in Supplementary Table 8.

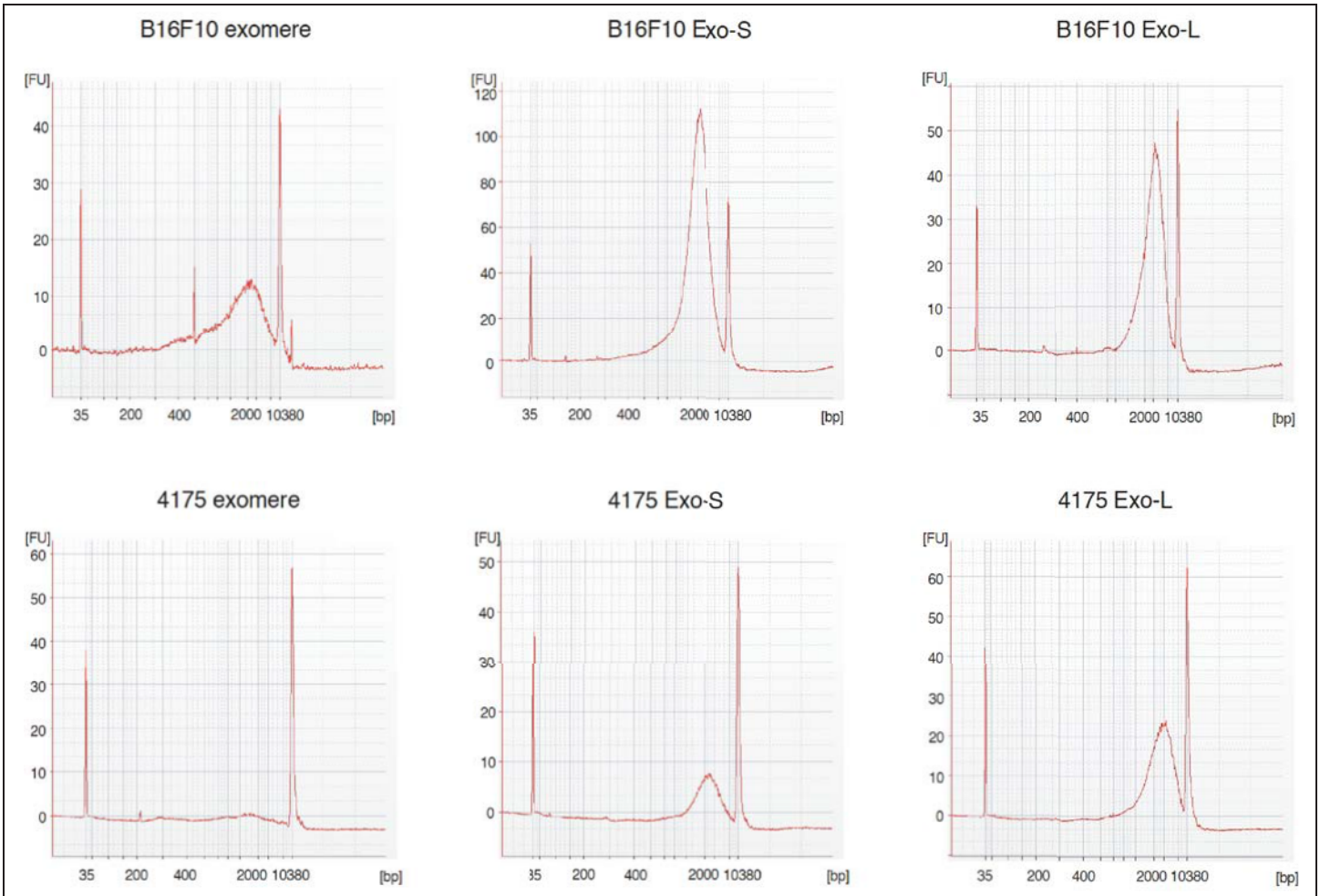

Supplementary Figure 6

Bioanalyzer analysis of the size distribution of DNA associated with exomere, Exo-S and Exo-L derived from B16F10 (top) and MDA-MB-4175 (bottom).

This experiment was repeated twice independently with similar results.

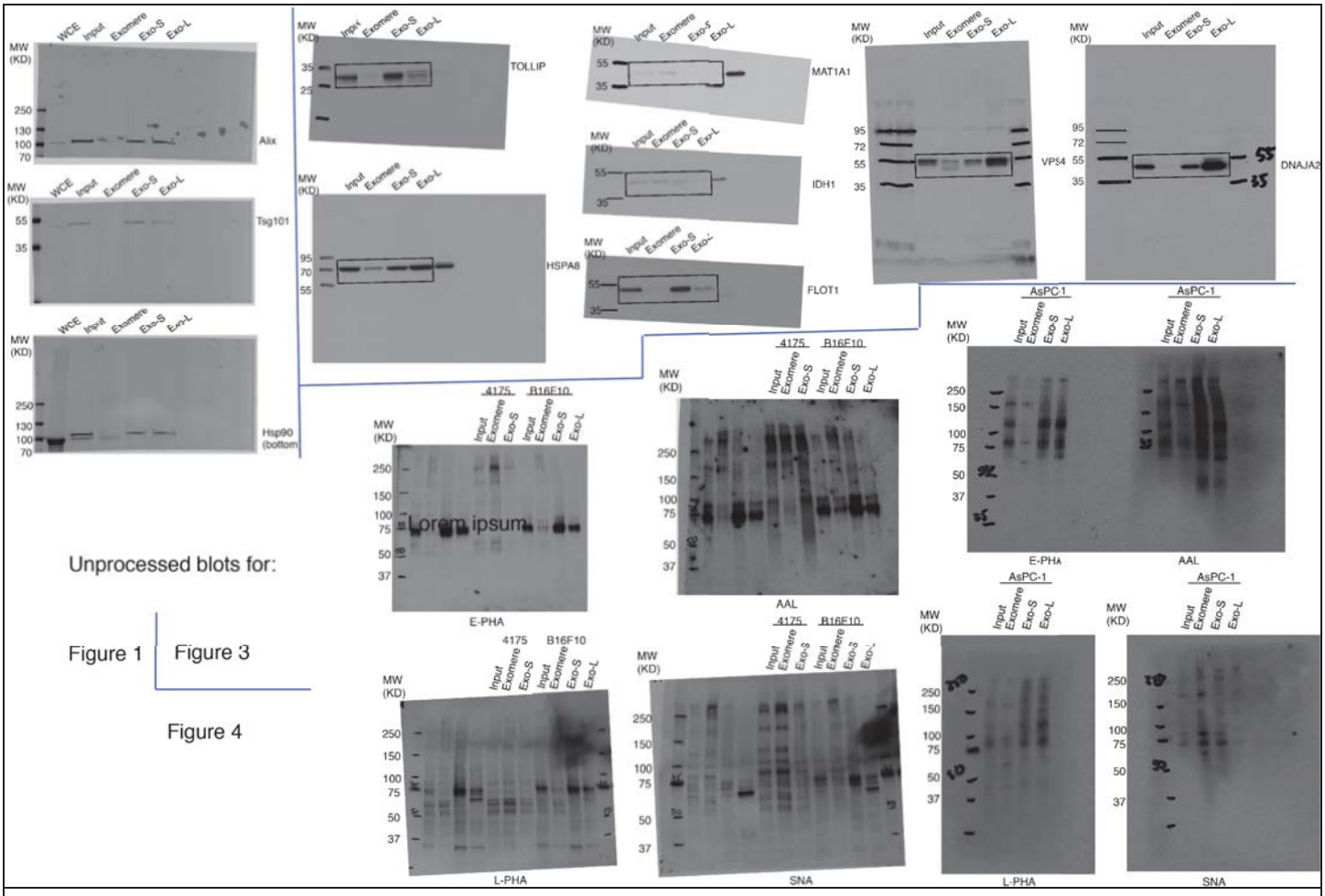

Supplementary Figure 7

Unprocessed blots for related figures in Figure 1, Figure 3 and Figure 4.

Supplementary Table 1. Types of cancer and corresponding cell lines examined for exosome subpopulations by AF4.

Supplementary Table 2. Complete list of proteins identified by proteomic mass spectrometry analysis of exomeres, Exo-S and Exo-L subpopulations derived from various cancer cell lines.

Supplementary Table 3. Subcellular localization of proteins associated with exomeres, Exo-S and Exo-L revealed by GSEA. Shown are top 19 pathways from a total of 580 gene sets derived from the gene ontology cellular components (http://software.broadinstitute.org/gsea/msigdb/genesets.jsp?collection=CC). For GSEA, a total of 30 samples (3 nanoparticle subtypes derived from 5 different cell lines; and two independent biological replicates for each nanoparticle samples) were subjected for statistical analysis. Kolmogorov-Smirnov statistic was calculated to evaluate whether proteins from a pre-determined pathway are significantly overrepresented towards the top or bottom of the ranked gene list.

Supplementary Table 4. Lists of proteins that are uniquely associated with or among the top 50 most abundant proteins in exomere, Exo-S and Exo-L derived from different cancer cell lines. For proteomic analysis, a total of 30 samples (3 nanoparticle subtypes derived from 5 different cell lines; and two independent biological replicates for each nanoparticle samples) were subjected for statistical analysis. Proteins were sorted by signal-to-noise statistic, (IJA - IJB)/(aA + aB) where IJ and a represent the mean and standard deviation of proteomic expression, respectively. The cutoff to select fraction-specific markers was fold change $\geq$5, false discovery rate (FDR) <0.05, and mean protein expression $\geq 10^8$ with the positivity in $\geq$80% (i.e. at least 4 out 5 samples from 5 different cell lines for each subset of nanoparticles) of the corresponding fraction.

Supplementary Table 5. Proteomic analysis of proteins associated with HDL, LDL and VLDL and survey of exomere proteins for subunits of known protein complexes.

Supplementary Table 6. GSEA of proteins associated with exomeres, Exo-S and Exo-L derived from various cancer cell lines. For GSEA, a total of 30 samples (3 nanoparticle subtypes derived from 5 different cell lines; and two independent biological replicates for each nanoparticle samples) were subjected for statistical analysis. Kolmogorov-Smirnov statistic was calculated to evaluate whether proteins from a pre-determined pathway are significantly overrepresented towards the top or bottom of the ranked gene list (FDR q <0.25).

Supplementary Table 7. Lipid classes identified in exomeres and exosome subsets derived from different cell lines.

Supplementary Table 8. Statistics Source Data. Source data for Fig. 1e, 1g, 2a-b, 2d, 4c, 5a-b, 6a-b, 7b and Supplementary Fig. 1b, 1d, 4c, 5c-d.